Choudhry RS, Khan KA, Khan SZ, Khan MA, Hassan A, Micromechanical modeling of 8-harness satin weave glass fiber-reinforced composites, Journal of Composite Materials, Volume 61, Issue 5, Pages 705 – 720.

Micromechanical Modeling of 8-Harness Satin Weave Glass Fiber Reinforced Composites

R. S. Choudhry[1,2,5], Kamran A. Khan[3*], Sohaib Zia Khan[4], Muhammad Ali Khan[4], Abid Hassan[5]

[1] Department of Mechanical Engineering, Capital University of Science and Technology, Islamabad, Pakistan
[2] National Composites Certification and Evaluation Facility, University of Manchester, Manchester, UK
[3] Department of Aerospace Engineering, Khalifa University of Science, Technology and Research (KUSTAR), Abu Dhabi, UAE
[4]Department of Engineering Sciences, National University of Sciences and Technology, Karachi, Pakistan
[5]Department of Mechanical Engineering, National University of Sciences and Technology (NUST), Islamabad, Pakistan

*Corresponding author: kamran.khan@kustar.ac.ae

Abstract

This study introduces a unit cell (UC) based finite element (FE) micromechanical model that accounts for correct post cure fabric geometry, in-situ material properties and void content within the composite to accurately predict the effective elastic orthotropic properties of 8-harness satin weave glass fiber reinforced phenolic (GFRP) composites. The micromechanical model utilizes a correct post cure internal architecture of weave, which was obtained through X-ray microtomography (XMT) tests. Moreover it utilizes an analytical expression to up-date the input material properties to account for in-situ effects of resin distribution within yarn (the yarn volume fraction) and void content on yarn and matrix properties. This is generally not considered in modeling approaches available in literature and in particular it has not been demonstrated before for FE micromechanics models of 8-harness satin weave composites. The UC method is used to obtain the effective response by applying periodic boundary conditions. The outcome of the analysis based on the proposed model is validated through experiments. After validation, the micromechanical model was further utilized to predict the unknown effective properties of the same composite.

Keywords: micromechanical model, homogenization, 8-harness satin weave, fiber reinforced composites, textile composites, X-ray microtomography.

1. Introduction

Woven fabrics are one of the most commonly used reinforcement for polymeric composites and find application in a variety of situations that require better shear and delamination resistance, impact resistance and biaxial strength ([1],[2]). They offer easier handling than unidirectional (UD) composite counterparts, have more balanced properties in a single layer as they combine two orientations and have relatively lower fabrication cost. They do however suffer from reduced strength as compared to an orthotropic (0/90) laminate due to fiber crimping. In this regard satin weaves with a high harness number (such as 8 harness satin weave) offer an attractive alternative to plain weaves as they have much reduced crimp, low porosity and better draping ability due to the fact that yarn interlacement takes place at every n^{th} pass (harness) of warp or weft yarn [2]. This comes at the cost of slightly poor stability, however, and thus necessitate their use in the form of pre-pregs to avoid weave distortion [1].

One factor that reduces the acceptability of satin weaves in practice, (especially for small manufacturers in developing economies as they do not have the means to fully characterize these materials using experimental methods) is the lack of effective material property data, which is required for design and finite element (FE) analysis of composite structures. Both analytical and FE micromechanics provides a recipe for calculating these effective properties without actually performing the experiments. The accuracy of such analysis depends on the soundness of the model.

Analytical micromechanical models based on simplified microstructural geometries of composites have been proposed to obtain effective mechanical properties, mainly for particle and unidirectional fiber re-inforced composites. Detailed discussion of various such micromechanical

models and bounds on the effective mechanical properties can be found in Aboudi [3], Khan and Muliana [4], Mura [5] and Nemat-Nasser and Hori [6].

Woven composites are generally considered more difficult to model analytically due to the complex weave architecture. Despite this researchers have developed analytical models based on elasticity theory to obtain their elastic properties (Chamis and Sendeckyj [7]). Ishikawa & Chou [8] are considered to be the pioneer who developed analytical models to predict the properties of woven composites. Based on laminate theory, they developed mosaic model [8] ignoring undulation and continuity of the yarns, a fiber crimp model accounting undulating portion of the yarn [9] and a bridging model explicitly for satin weave reinforced composites [10]. These models provided reasonable results but prediction were limited. Following Ishikawa & Chou [2], [8]–[10], various analytical models were proposed to obtain elastic properties of plain weave textile composites. For example, Naik & Shembekar [11], Naik & Ganesh [12], Vandeurzen, Ivens, & Verpoest [13], [14], Dimitrienko [15], Bystrom, Jekabsons, & Varna [16], Adumitroaie & Barbero [17]-[18] and Turner [19]. These models represented the woven geometry using two layers of yarns with homogenized properties for each layer considering the effects of yarn undulation. In order to predict the effective properties of complex fiber architecture, Searles, Odegard, & Kumosa [1] developed a simplified micro to meso scale analytical model. However, the actual geometry of 8-Harness satin weave was not reflected by the representative volume element (RVE) developed in their research. Most of the analytical models involve certain assumptions about the woven geometry as well as the constitutive relations of yarn and matrix due to the fact that complex mathematical models are required to capture the true geometry of undulating yarns and their interaction with the matrix portion of the composite.

Finite Element based micromechanical analysis can be applied to any type of woven architecture and they generally provide the best estimates of effective properties [20]. In micromechanical-FE

modeling approach a unit-cell (UC) model is introduced based on a RVE, which can be found in Aboudi [3], [21], Haj-Ali et al. ([22], [23]). The UC method is computationally efficient and allow to model and predict the overall composite responses with complex microstructural geometries. This method is suitable for incorporating stress, temperature, and other field dependent constituent properties at multiple length-scales.

Several micromechanical FE-homogenization schemes are proposed to calculate effective elastic characteristics of textile composite mainly for plain weave composites, for example., Dasgupta, Agarwal, & Bhandarkar [24], S. Li [25], Li & Wongsto [26], Tarfaoui & Akesbi [27], Boisse, et al. [28] Tabiei & Yi [29], Sherburn [30], Adumitroaie & Barbero [31], Whitcomb et al. [32] and Boisse et al. [33]. The effects of a volume fraction of the fiber on elastic properties were also highlighted in the literature [18]. Besides this the micromechanical models have also been used to predict the effective thermal conductivities of woven fabric composites (see for example Kyeongsik & Nam [34] and Farooqui [35]).

The review above highlights that limited micromechanical models are available for analyzing the orthotropic elastic properties of 8-satin weave composite as most of the work is related to plain weave composites. Available FE based micromechanical studies on 8-satin weave composites are limited due to three reasons. Firstly the yarn is usually modelled as a homogenous solid with input material properties independent of the manufacturing process parameters such as consolidation pressure, resin viscosity and heating rate. Secondly, the exact post cure/manufacture geometry of the weave is not considered. Thirdly, the effect of void content on yarn and matrix properties is ignored. In recent studies, for different weaves, it has been shown that it is important to consider the first two factors (see [36], [37], [17], [18], [31]). Owing to the inherent low stability of satin weave, it is expected that the manufacturing process parameters will have a profound effect on, the post cure internal architecture, volume fraction within yarn

and the void content. This will in turn effects the elastic properties of composite. Hence to study the effect of these parameters on effective properties of 8-satin weave composites, this study presents a FE based micromechanical model that not only takes into account the correct post cure 3D architecture (geometry) of weave in the composite using X-ray microtomography (XMT) but also accounts for the volume fraction within yarn and the reduction in composites effective properties due to the presence of voids. The latter is done on the basis of modification of input properties using empirically derived analytical expressions. Such detailed exposition based on FE micromechanical analysis, to the best of author's knowledge, has not been reported before for 8 harness satin weave.

2. Experimental Work

Three types of experimental tests were carried out, these are

i. Mechanical property testing (Tensile and shear tests) (Section 2.1 and 2.2)
ii. Non-destructive evaluation of UC architecture of cured composite using XMT (Section 2.3)
iii. Physical property characterization (volume fraction and void content) (Section 2.4)

2.1. Tensile Tests

The tensile tests were performed on composite (Primco SL246/40) as per the specifications set out in ISO 527-4:1997 (BS 2782-3) [38]. Primco-SL246/40 is an 8-harness satin weave glass fiber phenolic resin prepreg. (8 harness satin weave glass fabric pre-impregnated with modified phenolic resin mix to a nominal 40% resin content). The specimens were cut from a panel made of 6 layers of prepreg, cured using Quickstep™ [39] with a 0/0 (anti-symmetric) layup. End tabs made of aluminium were used to prevent failure in the jaws. On two of the specimens strain gauges (4 on each) were fitted to enable Poisson's ratio calculation, for the rest only the displacement along the tensile force axis was measured using extensometer. A summary of the

Formatted: Space Before: 6 pt, After: 6 pt

results of these tests is presented in Table 1. These values are later used for validating the outcome of FE micromechanics analysis. The graph in Figure 1 shows the experimental setup and stress strain graph for one of the test cases for which strain gauges were used to measure the exact strains (Label T4E in Table 1).

Table 1 Summary of tensile test results

Label	Width (b) mm	Gauge Length (Lo) mm	Thickness (h) mm	Tensile Modulus (GPa)	Tensile Strength (MPa)	Load at Failure (kN)	Poisson's ratio
T1E	25.60	50.00	1.93	20.15	276.93	13.47	-
T2E	24.55	50.00	1.94	20.89	305.48	14.22	-
T3E	25.32	50.00	1.94	18.70	285.90	14.00	-
T4E	23.20	50.00	1.92	22.31	267.46	11.40	0.14

Formatted Table

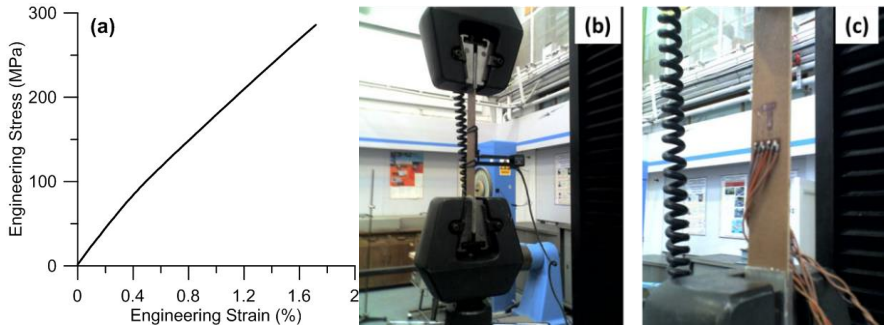

Figure 1. a) Tensile stress-strain curve for sample T4E. Setup of the apparatus used to measure tensile properties and Poison's ratio with (b) extensometer and c) strain gauges.

2.2. Shear Rail Tests

The in-plane shear modulus was obtained using the modified three rail shear test method (ASTM D 4225/D 4225M) [40]- [41]. The shear modulus for the linear range of shear stress – strain curve can be calculated using the chord modulus [41],

$$Gxy = G^{Chard} = \frac{\Delta \tau_{xy}}{\Delta \gamma_{xy}} \quad (1)$$

where G^{chord} = chord modulus of elasticity, Δ τ = difference in applied shear stress between the two strain points (noted from the stress-strain plot) used to define the chord modulus. Δ γ = difference between the two shear strain points (nominally 0.004). The shear strain was measured using eight strain gauges on each specimen. Four of these were installed on each face of the specimen. The strain gauges used were FCA 2-11 Tee rosettes. The strain at *ith* data point was measured using the equation given in ASTM D 4225/D 4225M [40],

$$\gamma_i = |\epsilon_{+45} - \epsilon_{-45}| \quad (2)$$

where γ_i = shear strain at *ith* data point, με , ε_{+45} = normal strain in the +45° direction at *ith* data point, $\mu\varepsilon$, ε_{-45} = normal strain in the –45° direction at *ith* data point, $\mu\varepsilon$. A stress - strain graphs for the specimens A and B along with the experimental setup for one of these tests is shown in Figure 2. Using the guidelines given in [41] we take the average of both experimental data to get shear modulus as shown in Table 2.

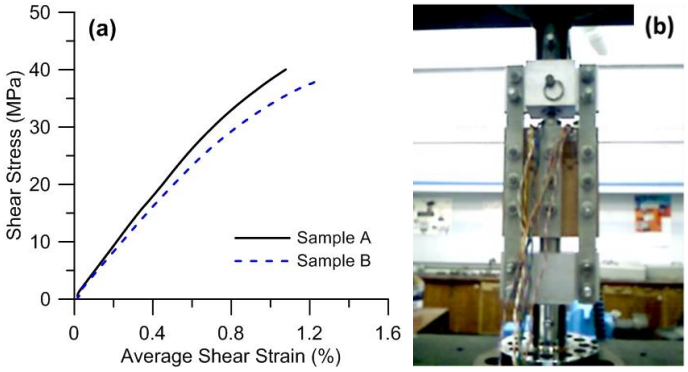

Figure 2 (a) Shear stress and strain data for specimen A and B (b) Three-rail shear test setup

Table 2. Test Results for two-rail shear tests

Modulus Specimen A	3.92 GPa
Modulus Specimen B	3.79 GPa
Average Modulus	**3.85 GPa**

2.3. X-ray microtomography

In literature, various techniques have been used to measure composite/fabric geometric parameters such as, scanning, optical microscopy, confocal microscopy, optical coherence tomography and XMT. XMT was found to be the best at non-destructively and clearly imaging the reinforcement microstructure of the entire sample in the final cured state and was not limited in depth [42]-[43]. In the present study, XMT images / slices are taken of the composite material whose properties were to be predicted numerically. Figure 3 shows X-ray microtomographic tomography setup and different views of the composite under investigation.

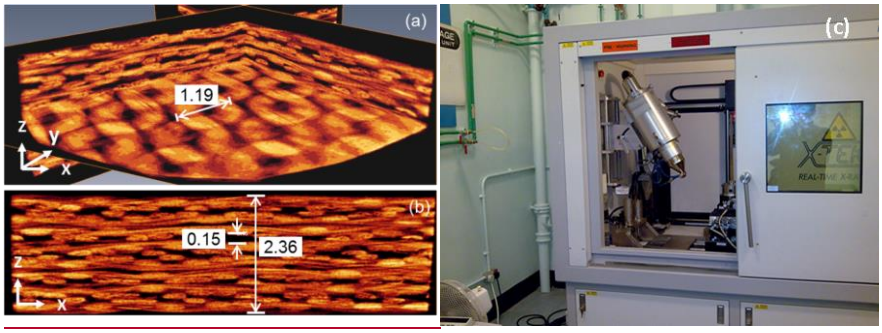

Figure 3. X-ray microtomographic images of 8-harness satin weave composite (Primco SL246/40), (a) multi-planer view of a specimen (b) XZ plane view of a specimen (c) X-ray tomography setup. (All Dimensions are in mm)

The Figure 3 (a) shows a superimposed multi-planar view, showing the XY, YZ and XZ planar views, where XY is the plane of laminate. In this image the XY plane is being shown through the centre of the laminate and hence both warp and weft fibre bundles can be seen. The image in

Figure 3 (b) shows a view in XZ plane for the same specimen and Figure 3 (c) shows X-ray tomography setup.

2.4. Physical property characterization tests

In developing FE micromechanics model of glass-fiber reinforced composites, generally, linearly-elastic-isotropic characteristics are considered for primary components (i.e., matrix and yarns) of the composite and it is customary to assume yarn to be homogenous. In reality, however, during the manufacturing process, the resin penetrates the yarn and after cure the yarn contains fibers as well as resin (matrix). The extent of interpenetration depends upon the fiber volume fraction, infiltration or vacuum pressure and resin viscosity during the initial phase of the cure cycle. In this study the specimens were made using Quickstep™ as opposed to Autoclave. The Quickstep™ process utilizes a much lower pressure as compared to autoclave, however it uses a much faster heating rate as opposed to autoclave. This generally results in a slightly higher void content and more resin infiltration within the yarn (promoted by a lower consolidation pressure and lower resin viscosity due to high ramp rate). Thus, effective properties for yarns which are required as an input to the micromechanics model also tend to vary accordingly depending on the extent of resin infiltration in yarn during cure. Various analytical models, for example [44],[45]-[46] in literature co-relate the yarn's fiber volume fraction and void content with the effective material properties of yarn. In this regard, tests were performed to calculate the fiber volume fraction of the composite, void content of the composite and the fiber volume fraction within the yarn.

2.4.1. Density Measurement Test

Density measurement test was performed according to the ASTM standard D 792 – 08 [47]. Mettler Toledo - XS204 analytical Balance [48] was used to measure the density of the composite. The advantage of using this precision analytical balance is that it can directly

compute the density provided weight of the specimen in air and its weight in immersed condition is measured using this balance. The average density of the composite measured by using six unique specimens was found to be 1.595 g/cm^3 with standard deviation of 0.0088.

2.4.2. Volume Fraction Test

Volume fraction tests were performed according to ASTM standard D 3171-99 [49]. Table 3 presents the results of the volume fraction tests.

Table 3. Results of volume fraction test for the composite.

Measurement	Mean Volume Fraction (6 Test Specimens)	Standard Deviation
Volume Fraction of Fibers (V_{fe})	39.9%	0.522
Volume Fraction of Matrix (V_m)	54.8%	0.917
Void Content (V_o)	5.3%	0.629

2.4.3. Fiber Volume Fraction Calculations

The yarns of the finalized geometric UC were modeled as solid volumes, however, these solid volumes cannot be fully comprised of fibers. This is due to the fact that resin flows into the yarns in almost all the situations [31]. The yarns are composed of fibers as well as matrix content as shown in Figure 4. The fraction of the fibers present in a yarn is defined as the fiber volume fraction of the yarn.

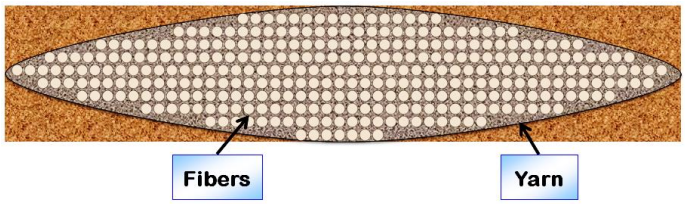

Figure 4. The fibers in a yarn of lenticular cross-section

To calculate the volume fraction of the composite, let V_{fe} be the experimental volume fraction of the fiber then the fiber volume fraction in the yarn, i.e., V_{fy} may be found out using the following relations

$$V_f = V \times V_{fe} \quad (3)$$

$$V_{fy} = \frac{V_f}{V_y} \quad (4)$$

Where V,V_y, V_f , V_{fy} are the volume of UC, volume of yarns in UC, volume of fibers in the UC and fiber volume fraction of the yarn, respectively.

The volume of the yarns in the UC was calculated by assuming a lenticular shape of the yarn. The reason of lenticular shape is explained in Section 3. Geometrically, the lenticular shape is formed by the intersection of two circles that are vertically offset by certain distances. These intersecting circles may either have different radii (r_1, r_2) to produce distorted lenticular or equal radii (r_1=r_2) to form symmetric lenticular cross-sections. Radii of circles (r_1, r_2) and offset distances (O_1=O_2=O) were evaluated by using the measured width 'w' and height 'h' of the yarn [30]. For symmetric lenticular cross-section

$$R = r_1 = r_2 = (w^2 + h^2) / 4h \quad (5)$$

$$O = 2R - h$$

Area of the lenticular yarn was calculated from the following relationships:

Area of the yarn = $A_y = A_1 + A_2 - A_3$

$$A_1 = A_2 = R^2 \cos^{-1}[\frac{O}{2R}] \quad \text{(since } r_1=r_2\text{)} \quad (6)$$

$$A_3 = \frac{1}{2}\sqrt{(2R-0)(2R+0)0^2} \quad (7)$$

Finally, the volume of the lenticular yarn was calculated by simply multiplying the area with the length of corresponding yarn. Table 4 shows the computed fiber volume fraction of the yarn and volume of the fiber and yarn in the UC.

Table 4. The fiber volume fraction within the yarn of the composite.

Parameter	Calculated Value
Volume of fibers in the UC (V_f)	1.472 mm^3
Volume of yarns in the UC (V_y)	1.895 mm^3
Fiber volume fraction of the yarn (V_{fy})	0.7768

3. Model Details

3.1. Geometric Modeling

The development of an accurate geometric model is critical in all numerical studies due to the fact that the reliability of the numerical results is governed by the accuracy of their respective geometric model. Keeping it in view, measurements taken from the XMT images of the composite are utilized to create a realistic geometric model. This geometric model will be further utilized to develop a micromechanical model whose numerical simulation will provide the material characterization of the composite.

3.1.1. Selection of Representative Volume Element (RVE)

Generally, the term UC is used as an alternative to RVE for periodic composites. In this study, XMT images are utilized to identify the repetitive pattern (UC) in the given composites. The UC as shown in Figure 5 includes 8 warp yarns and 8 weft yarns interlaced in a particular arrangement. The XMT slices (see for example Figure 5) highlight a key point that during manufacturing process due to the consolidation pressure the individual yarns of the satin weave within a lamina move slightly out of plain (i.e. in through thickness direction). Due to this reason if one uses the planar (XY) view slice for calculation of UC it appears as if the harness count is five instead of expected eight.

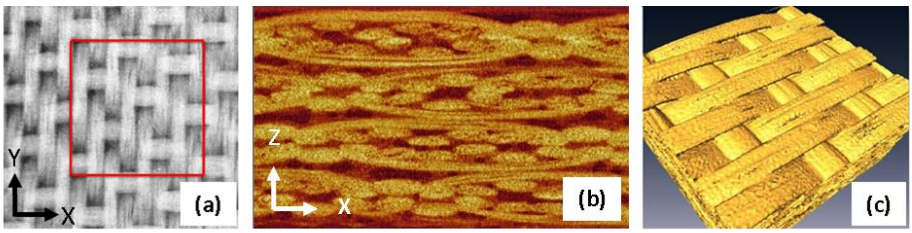

Figure 5. Identification of the UC for 8-harness satin weave (8/5/1) from XMT slice. (a) XY View (b) XZ View and (c) 3D view

A schematic representation of UC identified from XMT images is shown in Figure 6. This shows that this is 8/5/1 (harness/shift/interlacing) composite. Here 'W1 to W8' represent the warp and 'F1 to F8' represent the weft / fill yarns.

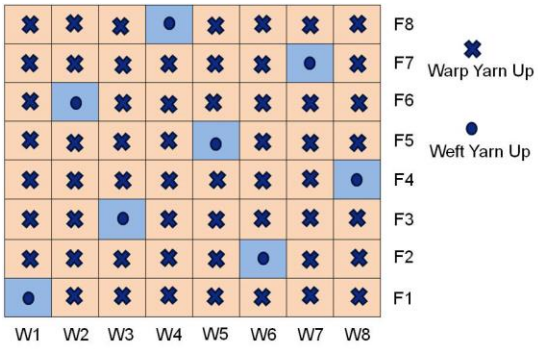

Figure 6: Schematic representation of UC for 8-harness satin weave (8/5/1)

3.1.2. Yarn Geometric parameters

A detail inspection of the XMT images of the composite is shown in Figure 7. Such observations revealed that a lenticular cross-section represents the true yarn geometry in our case. Thus, we used the lenticular shape to recreate the yarn geometry for the generation of UC. As explained earlier with reference to Figure 5, the yarns (lenticulars) were not perfectly aligned in the Z-axis, however, in this study they were modelled as perfectly aligned. It was assumed that the little out of plane miss-alignment in the actual specimen would not adversely affect the results because the overall UC dimensions were kept same as the average dimensions measured from XMT slices at

various locations within the specimen. ImageJ software [50] has been utilized to measure various UC related parameters (like yarn length, width, height, domain size, resin interface measurements etc.) from XMT images. Figure 8 shows a typical example of our measurement of yarn lengths and widths along warp as well as weft direction using XMT slice.

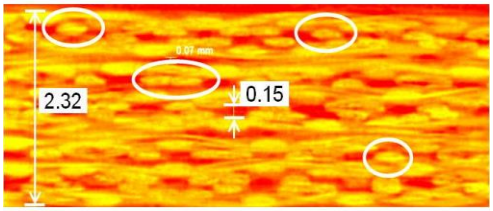

Figure 7: A lenticular cross-section shape of yarns visible in XMT slice.

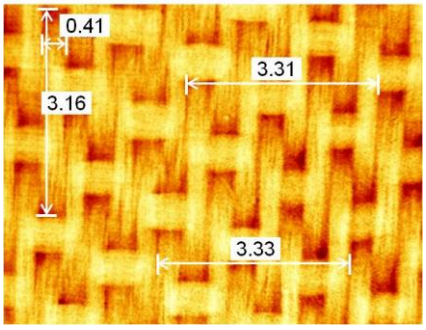

Figure 8: Measurement of yarn parameters from XMT slice using ImageJ software.

Other parameters like domain size for the UC and the measurements of resin interface between consecutive yarns were also obtained by analyzing the available XMT images. A typical measurement example is shown in Figure 9.

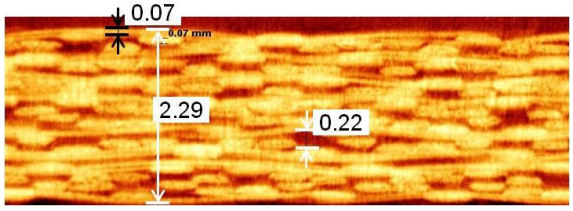

Figure 9: Measuring parameters for UC geometric model

The measured mean values from various samples are presented in Table 5. These values were further used in the development of a realistic model for 8-harness satin weave geometry.

Table 5: Yarn measurements from XMT images for the geometric model

Measurement	Mean (mm)	No. of Samples
Width of warp yarn	0.41	7

Width of weft yarn	0.45	7
Resin interface between consecutive yarns	0.01	5
Height of yarns	0.12	5
Thickness of resin layer between two consecutive lamina	0.05	5

3.1.3 8-Harness Satin Weave UC

In developing the UC it was assumed that both constituent materials are assumed to be consistent (free of cracks etc.) and perfectly bonded to each other before and after loading to comply with the basic requirement of strain compatibility in the theory of elasticity. Moreover the yarn was geometrically modelled as homogenous solid with a lenticular shape and the effect of relative distribution of constituents and geometry of fibers within the yarns was accounted for in terms of effective material properties of the yarn (section 4.2.2).

TexGen is a geometric modeling software for generating realistic geometries of textile composites [51], [52]. Using the measured properties in Section 3.1.2, considering a lenticular cross section shape for the yarn and following a suitable method in TexGen for defining the yarn path, undulation, repeats, intersection and orientation, we get the realistic geometrical model. The yarn orientations are required to correctly assign the properties to warp and weft yarns in the FE model. Figure 10 shows the UC after incorporating all the measured parameters essential for the true geometric reconstruction of the 8-harness satin weave UC.

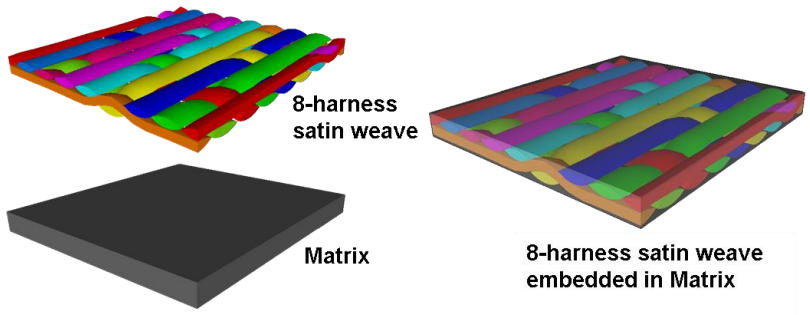

Figure 10: 8-harness satin weave composite UC for FE analysis.

4. Finite element analysis

In order to calculate the effective properties of the 8-harness satin weave UC, the FE analysis are performed using the commercial FE software Abaqus™.

4.1. Governing equations

We assume that the UC is subjected to quasi-static loading and undergoes small deformations. The UC satisfies the conservation of mass and momenta equations, which in absences of body force, body couple and inertial effects can be written in tensor notation as: $\dot{\rho} = 0$, $\sigma_{ij,j} = 0$, $\sigma_{ij} = \sigma_{ji}$ where ρ and σ_{ij} denote the mass density and the scalar components of the Cauchy stress tensor, respectively and the operator $(\ )_{,j} = \frac{\partial}{\partial x_j}$. The infinitesimal symmetric strain tensor is given by $\varepsilon_{ij} = \frac{1}{2}\left(u_{i,j} + u_{j,i}\right)$, where $u_{i,j}$ is the displacement gradient.

4.2. Constitutive model

The generalized Hooke's law relating stresses (σ_{ij}) and strains (ε_{kl}) can be written as ([21])

$$\sigma_{ij} = C_{ijkl}\varepsilon_{kl} \tag{8}$$

Here C_{ijkl} are the components of the fourth-order elasticity tensor. Isotropic materials (matrix in this study) require two independent material constants (E_m, ν_m), transversely isotropic materials (yarn in this study) needs five independent material constants and materials with orthotropic symmetry (i.e., the 8-harness satin weave UC) needs nine independent material parameters to define the material elastic response. For linear elastic materials, the constitutive relation can also be written in another form, i.e., $\varepsilon_{ij} = D_{ijkl}\sigma_{kl}$ with $D_{ijkl} = \left[C_{ijkl}\right]^{-1}$ as the components of the compliance tensor.

4.2.1. Orthotropic materials (UC effective response)

For materials with orthotropic symmetry, the stress and strain are expressed as [53]

$$\begin{Bmatrix} \varepsilon_{xx} \\ \varepsilon_{yy} \\ \varepsilon_{zz} \\ \varepsilon_{yz} \\ \varepsilon_{zx} \\ \varepsilon_{xy} \end{Bmatrix} = \begin{bmatrix} \frac{1}{E_x} & -\frac{\nu_{yx}}{E_y} & -\frac{\nu_{zx}}{E_z} & 0 & 0 & 0 \\ -\frac{\nu_{xy}}{E_x} & \frac{1}{E_y} & -\frac{\nu_{zy}}{E_z} & 0 & 0 & 0 \\ -\frac{\nu_{xz}}{E_x} & -\frac{\nu_{yz}}{E_y} & \frac{1}{E_z} & 0 & 0 & 0 \\ 0 & 0 & 0 & \frac{1}{2G_{yz}} & 0 & 0 \\ 0 & 0 & 0 & 0 & \frac{1}{2G_{zx}} & 0 \\ 0 & 0 & 0 & 0 & 0 & \frac{1}{2G_{xy}} \end{bmatrix} \begin{Bmatrix} \sigma_{xx} \\ \sigma_{yy} \\ \sigma_{zz} \\ \sigma_{yz} \\ \sigma_{zx} \\ \sigma_{xy} \end{Bmatrix} \tag{9}$$

Where $\frac{\nu_{yz}}{E_y} = \frac{\nu_{zy}}{E_z}, \frac{\nu_{zx}}{E_z} = \frac{\nu_{xz}}{E_x}, \frac{\nu_{xy}}{E_x} = \frac{\nu_{yx}}{E_y}$ (10)

4.2.2. Transversely isotropic materials (Yarn effective response)

As described earlier in Section 2.4 the fiber volume fraction of composite, the void content and the fiber volume fraction of yarn plays a critical role in determining the effective properties of the composite. Since the finite element model used in the study represents the yarns geometrically as homogenous continuum rather than discrete fibers with resin in between, an analytical model is required to calculate the correct effective yarn properties. Thus in this section an analytical model is presented to compute the homogenized properties of the yarn accounting for the fiber volume fraction within the yarn. Transverse isotropic symmetry conditions are considered for effective yarn characteristics and relationships are defined for each of the elastic constants to predict its true value corresponding to the evaluated fiber volume fraction. Figure 11 shows that in the yarn coordinate system, the lenticular yarn which comprises of matrix and

continuous fibers, is analogous to a UD composite; thus, we assume that the relationships defined in the literature for UD composites can be readily utilized to update yarn characteristics.

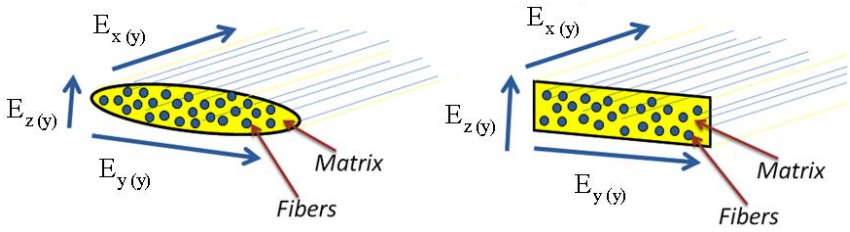

Figure 11: Analogy between Yarn (Left) and UD composite (Right)

Thus based on the UD analogy the yarns transverse properties can be evaluated using the relations listed in Table 6.

Table 6: Calculations of effective input properties of yarn

Parameter	**Equation**	**Theory used**
Longitudinal modulus $E_{x(y)}$	$E_{x(y)} = E_m + V_{fy}\,(E_f - E_m)$	Rule of mixtures [54]
Transverse modulus of the yarn $E_{y(y)} = E_{z(y)}$	$E_{y(y)} = E_{z(y)} = Em\,[\frac{1+\varsigma\eta(V_{fy})}{1-\eta(V_{fy})}]$ $\eta = \frac{(E_f/E_m)-1}{(E_f/E_m)-\varsigma}$ with $\varsigma = 2$	Halpin-Tsai [44]
In-plane shear modulus $G_{xy(y)} = G_{xz(y)}$	$G_{xy(y)} = G_{xz(y)} = G_m\,[\frac{(1+V_{fy})+(1-V_{fy})G_m/G_f}{(1-V_{fy})+(1+V_{fy})G_m/G_f}]$	Cylindrical assemblage model [46],[20]
Intra-laminar shear modulus $G_{yz(y)}$	$G_{yz(y)} = G_m\,[\frac{V_{fy}+\eta(1-V_{fy})}{\eta(1-V_{fy})+V_{fy}(G_m/G_f)}]$ with $\eta = \frac{3-4\upsilon_m+(G_m/G_f)}{4(1-\upsilon_m)}$	Stress partitioning parameter technique [20]
In-plane Poisson ratio $\upsilon_{xy(y)} = \upsilon_{xz(y)}$	$\upsilon_{xy(y)} = \upsilon_{xz(y)} = \upsilon_m + V_{fy}\,(\upsilon_f - \upsilon_m)$	Rule of mixtures [54]
Out-of-plane Poisson ratio $\upsilon_{yz(y)}$	$\upsilon_{yz(y)} = \frac{E_{y(y)}}{2(G_{yz(y)})} - 1$	Assumption of transverse isotropy

Formatted: Highlight
Formatted: Highlight

Where E_m, E_f, V_{fy}, υ_m and υ_f are the elastic modulus of the matrix, elastic modulus of the fiber, fiber volume fraction within cured yarn, Poisson ratio of the matrix and fiber, respectively.

4.3. Periodic Boundary Conditions (PBCs)

Globally the material consists of spatially repeated UCs (like the one shown in figure 10) and as a result, periodic boundary conditions (PBCs) are imposed on UC ([55]). Displacements, stresses and strains related to UC can be effectively handled using translational symmetry transformations [26]. These involve the identical transformation of stresses and strains in a particular UC to any other UC as their image. Relative displacements can also be transformed as macroscopic strains due to the similar nature of the two parameters. Following [26], mathematical relationships can be established for the relative displacement of a point P in a UC to the corresponding point $P^{/}$ (Figure 12) on the adjacent cell in terms of macroscopic strains.

$$u^{/} - u = (x^{/} - x)\,\varepsilon_x^{o} + (y^{/} - y)\,\gamma_{xy}^{o} + (z^{/} - z)\,\gamma_{xz}^{o} \quad (19)$$

$$v^{/} - v = (y^{/} - y)\,\varepsilon_y^{o} + (z^{/} - z)\,\gamma_{yz}^{o} \quad (20)$$

$$w^{/} - w = (z^{/} - z)\,\varepsilon_z^{o} \quad (21)$$

Where:

x, y, z = Coordinates of point P

u, v, w = Displacements at point P

$x^{/}, y^{/}, z^{/}$ = Coordinates of point $P^{/}$, the image of P

$u^{/}, v^{/}, w^{/}$ = Displacements at point $P^{/}$, the image of P

$\varepsilon_x^{o}, \varepsilon_y^{o}, \varepsilon_z^{o}, \gamma_{xy}^{o}, \gamma_{yz}^{o}, \gamma_{xz}^{o}$ = Macroscopic Strains defined in terms of virtual nodes

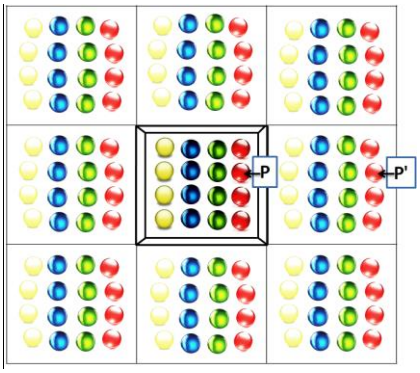

Figure 12: Schematic representation of point P and its corresponding image P/

Rigid body motions must be constrained and the displacement field defined by equations (19-21) may be applied as periodic boundary conditions (PBC) for the UC to analyze it numerically. In order to realize the periodic boundary conditions, discrete relationships must be written for the faces, edges as well as vertices of the UC. Detail expression for these PBC equations can be found in [26].

4.4. FE Homogenization

In defining boundary conditions, macroscopic strains are incorporated in the form of independent degrees of freedom. These independent degrees of freedom may also be considered as virtual nodes or master nodes in the language of commercial FE packages. Effective macroscopic stresses can be applied to the UC in terms of generalized concentrated loads applied at these virtual / master nodes. These generalized concentrated forces F_i (i.e. with the unit of force x length or N.m in SI system) have macroscopic strains as their work conjugate instead of displacement and thus these can be related to the macroscopic stresses through simple energy equivalence [26] given as follows: $\sigma_i^0 = F_i/V;\ where\ i = x, y, z, xy, xz\ and\ yz.$ V is the volume of the UC.

Formatted: Highlight
Formatted: Highlight
Formatted: Highlight

This procedure can be applied to each independent degree of freedom to obtain the corresponding relationship for macroscopic stresses in terms of generalized forces. To simplify the composite property computation process, a concentrated force equal to the volume of the UC may be applied to each macroscopic degree of freedom to directly evaluate the corresponding elastic constant from the displacement of the respective macroscopic degree of freedom. Effective elastic properties such as $E_x^0, E_y^0, E_z^0, G_{yz}^0, G_{zx}^0, G_{xy}^0, v_{xy}^0, v_{xz}^0$ and v_{yz}^0 may readily be predicted by simply inverting the corresponding macroscopic strain. Hence, the effective elastic properties can be evaluated using the following equations [26]

$$E_x^0 = \frac{\sigma_x^0}{\varepsilon_x^0} = \frac{F_x}{V\varepsilon_x^0};\ v_{xy}^0 = \frac{-\varepsilon_y^0}{\varepsilon_x^0};\ v_{xz}^0 = \frac{-\varepsilon_z^0}{\varepsilon_x^0} \qquad when\ F_y = F_z = F_{yz} = F_{zx} = F_{xy} = 0 \qquad (22)$$

$$E_y^0 = \frac{\sigma_y^0}{\varepsilon_y^0} = \frac{F_y}{V\varepsilon_y^0};\ v_{yx}^0 = \frac{-\varepsilon_x^0}{\varepsilon_y^0};\ v_{yz}^0 = \frac{-\varepsilon_z^0}{\varepsilon_y^0} \qquad when\ F_x = F_z = F_{yz} = F_{zx} = F_{xy} = 0 \qquad (23)$$

$$E_z^0 = \frac{\sigma_z^0}{\varepsilon_z^0} = \frac{F_z}{V\varepsilon_z^0};\ v_{zx}^0 = -\frac{\varepsilon_x^0}{\varepsilon_z^0};\ v_{zy}^0 = \frac{-\varepsilon_y^0}{\varepsilon_z^0} \qquad when\ F_x = F_y = F_{yz} = F_{zx} = F_{xy} = 0 \qquad (24)$$

$$G_{yz}^0 = \frac{\tau_{yz}^0}{\gamma_{yz}^0} = \frac{F_{yz}}{V\gamma_{yz}^0}; \qquad when\ F_x = F_y = F_z = F_{zx} = F_{xy} = 0 \qquad (25)$$

$$G_{zx}^0 = \frac{\tau_{zx}^0}{\gamma_{zx}^0} = \frac{F_{zx}}{V\gamma_{zx}^0}; \qquad when\ F_x = F_y = F_z = F_{yz} = F_{xy} = 0 \qquad (26)$$

$$G_{xy}^0 = \frac{\tau_{xy}^0}{\gamma_{xy}^0} = \frac{F_{xy}}{V\gamma_{xy}^0}; \qquad when\ F_x = F_y = F_z = F_{yz} = F_{zx} = 0 \qquad (27)$$

5. Results and Discussions

This section describes the model validation and results of various simulated cases. The micromechanical model was subjected to 'Sanity check' [26] before further analysis. This was done by setting the input properties for both constituents (i.e., matrix and yarns) of the UC equal to the matrix properties. The fact that we obtained a uniform stress distribution in the model and that the effective properties obtained are exactly in agreement to the input material data confirmed that the model was setup correctly. Next, we performed mesh independent studies by analyzing the parameters of interest (i.e., stresses, strains or displacements) against various mesh

sizes. A suitable mesh size is the one where the parameter of interest gets reasonably converged up to a steady value. The results of these will be discussed subsequently.

In this study we do the comparison of FE simulation outcomes with the experimental results for E_x^0 and G_{xy}^0 of 8-harness satin weave GFRP given in Table 1 and 2 of Section 2. In order to complete the elasticity tensor however, we will also predict the rest of the material parameters. Next, FE analysis of the UC are performed on three different cases of input properties. These cases clearly highlight the effect of incorporating volume fraction within yarn, on the numerical property prediction process. The input elastic properties of matrix and yarn are given in the following table.

Table 7: Constituents input properties for Case I, II and III. (Case I is yarn with 100% fiber in yarn; Case II is yarn with 77.68% fiber in yarn; Case III is 77.68% fiber in yarn and with void compensation for matrix properties)

	Material Parameter	Case I	Case II	Case III
Matrix	Modulus of Elasticity (E_m, GPa)	3.60	3.60	3.285
	Poisson Ratio (υ_m)	0.35	0.35	0.319
	Shear Modulus (G_m, GPa)	1.33	1.33	1.245
Yarn	Longitudinal Modulus of Elasticity ($E_{x(y)}$, GPa)	73	57.508	57.438
	In-plane Transverse Modulus of Elasticity ($E_{y(y)}$,GPa)	73	25.745	24.284
	Out-of-plane Transverse Modulus of Elasticity ($E_{z(y)}$,GPa)	73	25.745	24.284
	In-plane Poisson Ratio ($\upsilon_{xy(y)}$)	0.23	0.257	0.250
	Out-of-plane Poisson Ratio ($\upsilon_{xz(y)}$)	0.23	0.257	0.250
	Out-of-plane Poisson Ratio ($\upsilon_{yz(y)}$)	0.23	0.852	0.876
	In-plane Shear Modulus ($G_{xy(y)}$, GPa)	29.68	7.861	7.468
	Out-of-plane Shear Modulus ($G_{xz(y)}$, GPa)	29.68	7.861	7.468
	Out-of-plane Shear Modulus($G_{yz(y)}$, GPa)	29.68	6.949	6.472

Voxel based mesh independence studies were performed for the macroscopic strains [56]. While selecting the number of voxel count in x, y and z direction, it was ensured that length to thickness ratio of the elements do not exceed the permissible value i.e., $l / t < 10$ in order to avoid the distortion of elements. Voxel based meshes were generated using the strategy given in

Table 8. Numerical approximation for displacements may significantly vary in z-direction (through thickness) due to the effect of interlaced regions and undulation of yarns. Voxel count in z-direction, therefore, should be carefully altered while performing mesh independence studies.

Table 8: Voxel based meshing strategy

Voxel Count X	Voxel Count Y	Voxel Count Z	No. of Elements	Aspect Ratio
40	40	20	32000	6.12
50	50	25	62500	6.12
60	60	30	108000	6.12
70	70	30	147000	5.24
80	80	30	192000	4.59
80	80	40	256000	6.12

5.1. Case 1-Property Prediction without Considering Volume Fraction Effects

In this case, volume fraction effects within the yarn are totally ignored and the yarns are considered to be completely comprised of fibers (solid volumes) i.e., fiber volume fraction = 1. Moreover, the matrix (resin) portion is considered to be completely void free. Linearly-elastic-isotropic behavior is considered for both of the primary constituents and properties are given in Table 7. For Case 1, mesh independence studies were performed for the parameters of interest $\varepsilon_x{}^o$ and $\gamma_{xy}{}^o$ to numerically approximate the corresponding elastic moduli E_x^0 and G_{xy}^0. Mesh independence graphs presented below (Figure 13) clearly illustrate the convergence of results for a 192,000 element mesh.

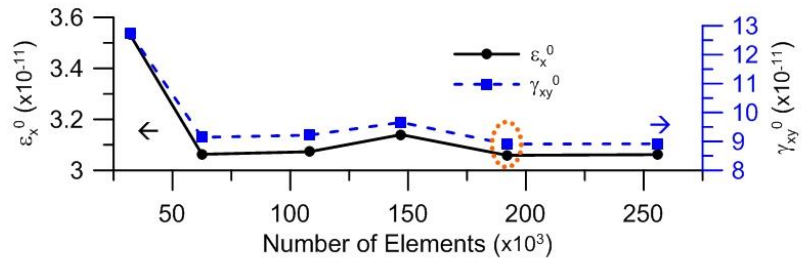

Figure 13: Mesh independence studies for Case 1

Table 9 compare the comparison of experimental data and the effective elastic moduli E_x^0 and G_{xy}^0 that were evaluated by taking the inverse of corresponding macroscopic strains $\varepsilon_x{}^o$and $\gamma_{xy}{}^o$ respectively for the converged mesh. The huge difference is observed between the numerical approximations and the experimental results.

Table 9: Comparison of results computed for Case 1

Elastic Moduli	Numerical Approximation	Experimental Value	% Difference
Modulus of Elasticity in Warp Direction, E_x^0	32.69 GPa	20.512 GPa	59.37 %
In-plane Shear Modulus, G_{xy}^0	11.225 GPa	3.855 GPa	191.18 %

5.2. Case 2-Property Prediction while Incorporating Volume Fraction Effects

In case 2, using the methodology illustrated in Section 4.2.2, yarn isotropic elastic properties were modified according to the calculated fiber volume fraction (i.e., 0.7768). Thus, the volume fraction effects were incorporated in the yarn input data. The void content present in the composite was still ignored for this case. Updated material input properties for Case 2 were given earlier in Table 7.

The updated yarn input properties are orthotropic therefore we performed voxel based mesh independence studies to select a suitably converged mesh for the following parameters of interest $\varepsilon_x{}^o$, $\varepsilon_y{}^o$, $\varepsilon_z{}^o$, $\gamma_{xy}{}^o$, $\gamma_{yz}{}^o$, $\gamma_{xz}{}^o$. Mesh independence trends for all theses parameters were carefully inspected in order to select a suitably converged mesh size for numerical approximations. It can be observed from mesh independence graphs that mesh was readily converged for the displacement of macroscopic degrees of freedom $\varepsilon_x{}^o$, $\varepsilon_y{}^o$ and $\gamma_{xy}{}^o$. However, for degrees of freedom $\varepsilon_z{}^o$, $\gamma_{yz}{}^o$ and $\gamma_{xz}{}^o$, the mesh was converged for a relatively large number of elements. It is due to the reason that yarn undulations in z-direction cause significant variation in through-thickness displacements as compared to the in-plane displacements. Considering a suitable

representative mesh size for all parameters, mesh was finalized with 192,000 C3D8 elements. Figure 14 shows the convergence of macroscopic strains for different mesh densities.

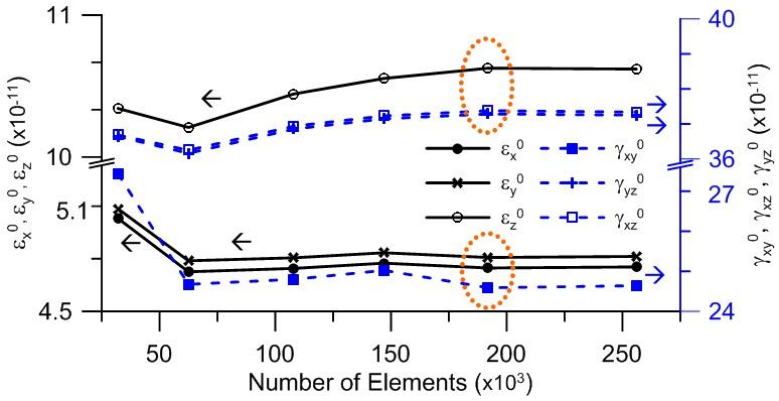

Figure 14: Mesh independence studies for Case 2

Comparison between computed results for Case 2 and available experimental data is presented in the Table 10. This table illustrates that by using the orthotropic effective representation for the yarn with the calculated fiber volume fraction, the difference in simulation and experiments reduces drastically. For many practical purposes such level of accuracy is considered sufficient.

Table 10: Comparison of results computed for Case 2

Elastic Moduli	Numerical Approximation	Experimental Value	% Difference
Modulus of Elasticity in Warp Direction, E_x^0	20.94 GPa	20.512 GPa	2.08 %
In-plane Shear Modulus, G_{xy}^0	4.066 GPa	3.855 GPa	5.47 %

5.3. Case 3-Property Prediction with Void Content Compensation

Elastic moduli predicted in Case 2 are slightly over-predicted than the available experimental results due to the assumption of considering a completely void free composite. During manufacturing process voids are distributed in the matrix region as well as within the fibers of the yarns but no firm relationship may be established to address the void content in the property

prediction process. Nonetheless, the author adopted a simple but workable methodology to incorporate the effects of this void content. Experimental results of the volume fraction enlightens us with the idea of associating void content with the input matrix properties. Since the matrix region is composed of resin as well as voids, the matrix input properties can simply be reduced in proportion to the fraction of the void content present in the matrix. From volume fraction test results presented in Section 2, void compensation factor (*Vcf*) may be calculated as; $Vcf = V_m / (V_m + V_o) = 0.9126$. where Vm is the volume fraction of matrix (resin) and Vo is the Volume fraction of void content.

Input matrix properties may be updated by simply multiplying them with above calculated value of the resin volume fraction. These updated matrix properties may then be utilized to calculate updated yarn input properties as per the procedure described in Section 4.2.2. Since the yarn input properties will be modified according to the void compensated matrix properties, the effect of voids present within the yarns will automatically get incorporated. Update input properties are presented in Table 7 considering the void compensation factor (Vcf = 0.9126) and fiber volume fraction of yarns (V_{fy} = 0.7768). The use of these modified input properties results obtained from FE homogenization method described earlier, was found to be in excellent agreement with the available experimental values for E_x^0 and G_{xy}^0 as shown in Table 11. Thus, the proposed method to cater for the void fraction effects proved effective as it gave promising material characteristics estimates.

Table 11: Comparison of results computed for Case ~~2~~3

Elastic Moduli	Numerical Approximation	Experimental Value	% Difference
Modulus of Elasticity in Warp Direction, E_x^0	20.33 GPa	20.512 GPa	0.89 %
In-plane Shear Modulus, G_{xy}^0	3.843 GPa	3.855 GPa	0.31 %

Since the numerical results for two of the elastic constants are validated, all the other unknown effective properties may then be reliably predicted using the same methodology. Predicted orthotropic properties are tabulated as follows:

Table 12: Effective orthotropic properties predicted in Case 3

Composite Effective Property	Numerical Approximation	Case 2
Modulus of Elasticity in Warp Direction, E_x^0	20.33 GPa	20.94 GPa
Modulus of Elasticity in Weft Direction, E_y^0	20.03 GPa	20.65 GPa
Out-of-plane Elastic Modulus, E_z^0	8.312 GPa	9.411 GPa
In-plane Shear Modulus, G_{xy}^0	3.843 GPa	4.066 GPa
Out-of-plane Shear Modulus, G_{zx}^0	2.504 GPa	2.675 GPa
Out-of-plane Shear Modulus, G_{yz}^0	2.510 GPa	2.682 GPa
In-plane Poisson Ratio, v_{xy}^0	0.16	0.17
In-plane Poisson Ratio, v_{yx}^0	0.15	0.17
Out-of-plane Poisson Ratio, v_{xz}^0	0.47	0.49
Out-of-plane Poisson Ratio, v_{zx}^0	0.19	0.22
Out-of-plane Poisson Ratio, v_{yz}^0	0.48	0.50
Out-of-plane Poisson Ratio, v_{zy}^0	0.20	0.22

Formatted Table

6. Conclusions

We proposed a micromechanical model to predict the effective orthotropic properties of 8-harness satin weave glass fiber reinforced phenolic (GFRP) composites. The input material properties of yarn are obtained by considering the fiber volume fraction effects due to resin infiltration and presence of voids. UC based on the real microstructure of composite is obtained using XMT images and modelled geometrically using TexGen. Periodic boundary conditions are imposed on the UC and finite element analysis are performed using Abaqus™ to obtain the effective response. Comparison of three different effective homogenization strategies for the numerical model in terms of input material data showed that the elastic material parameters

obtained from the FE simulation showed good agreement with the available experimental data for the case where the fiber volume fraction within yarn and voids content is accounted for analytically during the homogenization process. Thus, we conclude that in-order to correctly calculate the effective properties of 8 harness stain weave composites a realistic geometric model of cured composite is required. Moreover we also conclude that fiber volume fraction within the yarn and void content effects on elastic material properties can be accounted for analytically using the methodology described in this paper for the 8-harness satin weave composites.

ACKNOWLEDGEMENT

Authors are thankful for support of Henry Mosely Tomography Centre and the National Composites Certification and Evaluation Facility (NCCEF), University of Manchester, UK where all experimental tests were performed. They also gratefully acknowledge the British Council and Department for International Development (DFID), UK which funded the travel of authors to UK for the said experiments through the DelPHE 780 project grant.

REFERENCES

[1] K. Searles, G. Odegard, and M. Kumosa, "Micro- and mesomechanics of 8-harness satin woven fabric composites: I — evaluation of elastic behavior," *Compos. Part Appl. Sci. Manuf.*, vol. 32, no. 11, pp. 1627–1655, Nov. 2001.

[2] T. Ishikawa and T.-W. Chou, "Stiffness and strength behaviour of woven fabric composites," *J. Mater. Sci.*, vol. 17, no. 11, pp. 3211–3220, Nov. 1982.

[3] J. Aboudi, M.-J. Pindera, and S. M. Arnold, "Higher-order theory for functionally graded materials," *Compos. Part B Eng.*, vol. 30, no. 8, pp. 777–832, Dec. 1999.

[4] K. A. Khan and A. H. Muliana, "Effective thermal properties of viscoelastic composites having field-dependent constituent properties," *Acta Mech.*, vol. 209, no. 1–2, pp. 153–178, Apr. 2009.

[5] T. Mura, *Micromechanics of Defects in Solids*. Springer Science & Business Media, 2012.

[6] S. Nemat-Nasser and S. Hori, *Micromechanics: Overall Properties of Heterogeneous Materials, Second Edition*, 2 edition. Amsterdam ; New York: North Holland, 1999.

[7] C. C. Chamis and G. P. Sendeckyj, "Critique on Theories Predicting Thermoelastic Properties of Fibrous Composites," *J. Compos. Mater.*, vol. 2, no. 3, pp. 332–358, Jul. 1968.

[8] T. Ishikawa and T.-W. Chou, "Elastic Behavior of Woven Hybrid Composites," *J. Compos. Mater.*, vol. 16, no. 1, pp. 2–19, Jan. 1982.

[9] T.-W. CHOU and T. ISHIKAWA, "One-dimensional micromechanical analysis of woven fabric composites," *AIAA J.*, vol. 21, no. 12, pp. 1714–1721, 1983.

[10] T. Ishikawa, M. Matsushima, Y. Hayashi, and T.-W. Chou, "Experimental Confirmation of the Theory of Elastic Moduli of Fabric Composites," *J. Compos. Mater.*, vol. 19, no. 5, pp. 443–458, Sep. 1985.
[11] N. K. Naik and P. S. Shembekar, "Elastic Behavior of Woven Fabric Composites: I—Lamina Analysis," *J. Compos. Mater.*, vol. 26, no. 15, pp. 2196–2225, Dec. 1992.
[12] N. K. Naik and V. K. Ganesh, "An analytical method for plain weave fabric composites," *Composites*, vol. 26, no. 4, pp. 281–289, Apr. 1995.
[13] P. Vandeurzen, J. Ivens, and I. Verpoest, "A three-dimensional micromechanical analysis of woven-fabric composites: I. Geometric analysis," *Compos. Sci. Technol.*, vol. 56, no. 11, pp. 1303–1315, 1996.
[14] P. Vandeurzen, J. Ivens, and I. Verpoest, "A three-dimensional micromechanical analysis of woven-fabric composites: II. Elastic analysis," *Compos. Sci. Technol.*, vol. 56, no. 11, pp. 1317–1327, 1996.
[15] Y. Dimitrienko, "Modelling of the Mechanical Properties of Composite Materials at High Temperatures. Part 3. Textile Composites," *Appl. Compos. Mater.*, vol. 5, no. 4, pp. 257–272, Jul. 1998.
[16] J. Byström, N. Jekabsons, and J. Varna, "An evaluation of different models for prediction of elastic properties of woven composites," *Compos. Part B Eng.*, vol. 31, no. 1, pp. 7–20, Jan. 2000.
[17] A. Adumitroaie and E. J. Barbero, "Beyond plain weave fabrics – I. Geometrical model," *Compos. Struct.*, vol. 93, no. 5, pp. 1424–1432, Apr. 2011.
[18] A. Adumitroaie and E. J. Barbero, "Beyond plain weave fabrics – II. Mechanical properties," *Compos. Struct.*, vol. 93, no. 5, pp. 1449–1462, Apr. 2011.
[19] M. R. Turner, "Tow placement studies for liquid composite moulding," 1998. [Online]. Available: http://eprints.nottingham.ac.uk/12085/. [Accessed: 05-Nov-2015].
[20] E. J. Barbero, *Introduction to Composite Materials Design, Second Edition*. CRC Press, 2010.
[21] J. Aboudi, "Micromechanical analysis of the strength of unidirectional fiber composites," *Compos. Sci. Technol.*, vol. 33, no. 2, pp. 79–96, 1988.
[22] R. Haj-Ali, H. Kilic, and A.-H. Zureick, "Three-dimensional micromechanics-based constitutive framework for analysis of pultruded composite structures," *J. Eng. Mech.*, vol. 127, no. 7, pp. 653–660, 2001.
[23] R. M. Haj-Ali and A. H. Muliana, "A multi-scale constitutive formulation for the nonlinear viscoelastic analysis of laminated composite materials and structures," *Int. J. Solids Struct.*, vol. 41, no. 13, pp. 3461–3490, Jun. 2004.
[24] A. Dasgupta, R. K. Agarwal, and S. M. Bhandarkar, "Three-dimensional modeling of woven-fabric composites for effective thermo-mechanical and thermal properties," *Compos. Sci. Technol.*, vol. 56, no. 3, pp. 209–223, 1996.
[25] S. Li, "General unit cells for micromechanical analyses of unidirectional composites," *Compos. Part Appl. Sci. Manuf.*, vol. 32, no. 6, pp. 815–826, Jun. 2001.
[26] S. Li and A. Wongsto, "Unit cells for micromechanical analyses of particle-reinforced composites," *Mech. Mater.*, vol. 36, no. 7, pp. 543–572, Jul. 2004.
[27] M. Tarfaoui and S. Akesbi, "A finite element model of mechanical properties of plain weave," *Colloids Surf. Physicochem. Eng. Asp.*, vol. 187–188, pp. 439–448, Aug. 2001.
[28] P. Boisse, K. Buet, A. Gasser, and J. Launay, "Meso/macro-mechanical behaviour of textile reinforcements for thin composites," *Compos. Sci. Technol.*, vol. 61, no. 3, pp. 395–401, Feb. 2001.

[29] A. Tabiei and W. Yi, “Comparative study of predictive methods for woven fabric composite elastic properties,” *Compos. Struct.*, vol. 58, no. 1, pp. 149–164, Oct. 2002.
[30] M. Sherburn, “Geometric and Mechanical Modelling of Textiles,” 2007. [Online]. Available: http://eprints.nottingham.ac.uk/10303/. [Accessed: 06-Nov-2015].
[31] A. Adumitroaie and E. J. Barbero, “Stiffness and Strength Prediction for Plain Weave Textile Reinforced Composites,” *Mech. Adv. Mater. Struct.*, vol. 19, no. 1–3, pp. 169–183, Jan. 2012.
[32] X. Tang, J. D. Whitcomb, Y. Li, and H.-J. Sue, “Micromechanics modeling of moisture diffusion in woven composites,” *Compos. Sci. Technol.*, vol. 65, no. 6, pp. 817–826, May 2005.
[33] P. Boisse, B. Zouari, and J.-L. Daniel, “Importance of in-plane shear rigidity in finite element analyses of woven fabric composite preforming,” *Compos. Part Appl. Sci. Manuf.*, vol. 37, no. 12, pp. 2201–2212, Dec. 2006.
[34] K. Woo and N. S. Goo, “Thermal conductivity of carbon-phenolic 8-harness satin weave composites,” *Compos. Struct.*, vol. 66, no. 1–4, pp. 521–526, Oct. 2004.
[35] J. K. Farooqi, *Modelling thermal transport in woven ceramic matrix composites*. University of Manchester, 2007.
[36] S. D. Green, M. Y. Matveev, A. C. Long, D. Ivanov, and S. R. Hallett, “Mechanical modelling of 3D woven composites considering realistic unit cell geometry,” *Compos. Struct.*, vol. 118, pp. 284–293, Dec. 2014.
[37] S. R. Hallett and P. Biragoni, “Damage Prediction for 3D Woven Composite Structural Features,” presented at the 10th International Conference on Textile Composites (TEXCOMP 10), 2010.
[38] “Part 4: Test conditions for isotropic and orthotropic fibre-reinforced plastic composites, in Plastics - Determination of tensile properties.” BRITISH STANDARD, 1997.
[39] Coenen V, Hatrick M, Law H, Brosius D, Nesbitt A, Bond D., “A feasibility study of Quickstep processing of an aerospace composite material.” MPE-EUROPEconference proceedings, 2005.
[40] “Standard test method for in-plane shear properties of polymer matrix composite materials by the Rail Shear method, Designation: D4255/D 4255M-01.” American Society for Testing Materials (ASTM), 2002.
[41] S. M. Mohseni Shakib and S. Li, “Modified three rail shear fixture (ASTM D 4255/D 4255M) and an experimental study of nonlinear in-plane shear behaviour of FRC,” *Compos. Sci. Technol.*, vol. 69, no. 11–12, pp. 1854–1866, Sep. 2009.
[42] J. P. Dunkers, R. S. Parnas, C. G. Zimba, R. C. Peterson, K. M. Flynn, J. G. Fujimoto, and B. E. Bouma, “Optical coherence tomography of glass reinforced polymer composites,” *Compos. Part Appl. Sci. Manuf.*, vol. 30, no. 2, pp. 139–145, Feb. 1999.
[43] R. S. Choudhry, S. F. Hassan, S. Li, and R. Day, “Damage in single lap joints of woven fabric reinforced polymeric composites subjected to transverse impact loading,” *Int. J. Impact Eng.*, vol. 80, pp. 76–93, Jun. 2015.
[44] J. C. Halpin, “Effects of Environmental Factors on Composite Materials.,” Jun. 1969.
[45] H. T. Hahn and S. W. Tsai, *Introduction to Composite Materials*. CRC Press, 1980.
[46] Z. Hashin and B. W. Rosen, “The Elastic Moduli of Fiber-Reinforced Materials,” *J. Appl. Mech.*, vol. 31, no. 2, pp. 223–232, Jun. 1964.
[47] “ASTM D792 - 08 Standard test methods for density and specific gravity (relative density) of plastics by displacement, ASTM International: West Conshohocken, PA, USA.” .

[48] "http://us.mt.com/dam/LabTec/documents/excellence_balance/XS/Datasheet_brochure/11796113_XS_Analytical_DB_PF_EN_03_2010.pdf."
[49] "Standard Test Methods for Constituent Content of Composite Materials, Designation: ASTM D3171 - 99." .
[50] M. D. Abramoff, P. J. Magalhães, and S. J. Ram, "Image processing with ImageJ," *Biophotonics Int.*, vol. 11, no. 7, pp. 36–42, 2004.
[51] F. Robitaille, B. R. Clayton, A. C. Long, B. J. Souter, and C. D. Rudd, "Geometric modelling of industrial preforms: Woven and braided textiles," *Proc. Inst. Mech. Eng. Part J. Mater. Des. Appl.*, vol. 213, no. 2, pp. 69–83, Apr. 1999.
[52] F. Robitaille, A. C. Long, and C. D. Rudd, "Geometric modelling of textiles for prediction of composite processing and performance characteristics," *Plast. Rubber Compos.*, vol. 31, no. 2, pp. 66–75, Feb. 2002.
[53] J. N. Reddy, *An introduction to continuum mechanics*. Cambridge University Press, 2013.
[54] E. J. Barbero, *Introduction to Composite Materials Design, Second Edition*. CRC Press, 2010.
[55] F. Robitaille and R. Gauvin, "Compaction of textile reinforcements for composites manufacturing. I: Review of experimental results," *Polym. Compos.*, vol. 19, no. 2, pp. 198–216, Apr. 1998.
[56] T. Kanit, S. Forest, I. Galliet, V. Mounoury, and D. Jeulin, "Determination of the size of the representative volume element for random composites: statistical and numerical approach," *Int. J. Solids Struct.*, vol. 40, no. 13–14, pp. 3647–3679, Jun. 2003.